Korean J. Chem. Eng., 34(5), 1366-1376 (2017)
DOI: 10.1007/s11814-017-0037-x

pISSN: 0256-1115
eISSN: 1975-7220

Novel multi-scale diffusion model for catalytic methane combustion

Kai Huang†, Lianguang Wang, Yang Xu, and Dongfang Wu

School of Chemistry and Chemical Engineering, Southeast University, Nanjing 211189, P. R. China
(*Received 23 December 2016 • acceped 9 February 2017*)

Abstract−A multi-scale model of methane catalytic combustion was built by a series of balance equations and diffusion equations, and these equations were solved through the computational fluid dynamics (CFD) software. The difference between this work and previous model is the diffusion process in catalyst coating was considered. By analyzing the methane conversion, temperature distribution and mass fraction contours of every component, the performance of multi-scale model was compared with that of the pure CFD model without diffusion. The effects of diffusion, methane concentration, flow rate on the methane conversion and temperature distribution of monolithic reactor were also evaluated and discussed by the multi-scale model. The multi-scale model showed better accuracy than the pure CFD model without diffusion process. Different methane concentrations and gas flow rates had enormous effects on the methane conversion and temperature. Therefore, it was beneficial to the reaction process to adjust the methane concentration and gas flow rate appropriately.

Keywords: Multi-scale Model, Monolithic Reactor, Methane, Catalytic Combustion, CFD Simulation

INTRODUCTION

Methane catalytic combustion is an extremely attractive way in dealing with low-concentration methane; this way also enhances the combustion efficiency and avoids production of NO_x and other pollutants [1]. At the same time, the catalytic combustion temperature is lower than traditional flame combustion, and there is no combustion limit under catalytic combustion [2]. Methane is a kind of greenhouse gas [3] whose greenhouse effect is 21-times larger than CO_2 [4-6]. The application of methane catalytic combustion can be divided into two types: to provide heat and energy, and to obliterate low concentration methane [7]. In a coal mine, methane concentration is low so that flame combustion cannot get rid of low-concentration methane, which leads to serious global warming. Therefore, catalytic combustion is the best way to deal with low-concentration methane [8].

At present, two kinds of catalysts have been developed for methane catalytic combustion: noble metal catalyst and non-noble metal catalyst. The most representative noble metal catalyst has the active components of Pd and Pt, which are supported on the Al_2O_3, Si_3N_4 and other supports [9-12]. This kind of catalyst has higher catalytic activity and excellent anti-sulfur-poisoning property [13]. The typical non-noble metal catalysts include perovskite [14-16], hexaaluminate [17,18], pyrochlore [19] and metal complex, whose catalytic activity is lower than noble metal catalyst, but the thermostability of non-noble metal catalyst attracted the extensive attention of researchers. Hence, the catalyst supported by Pd showed the best performance for methane catalytic combustion [20,21] and it also had higher catalytic activity in lower temperature than other catalysts.

The monolithic reactor was widely used for methane catalytic combustion by previous scholars [22,23] because of its uniform channels and particular reactor characteristics: (1) lower pressure drop, (2) larger geometry of the specific surface area, and (3) uniform gas flow in the channels. All these features are beneficial to the process of methane catalytic combustion. The comparison of packed-bed reactor and structured reactor showed more advantages of monolithic reactor by Marín [24].

More and more reactor models for methane catalytic combustion have been built for optimization of reaction conditions and improving reactor properties, and computational fluid dynamics (CFD) simulation used for designing of many industrial processes [25-27]. Hwang [28] studied a kind of catalytic combustion reactor of mixed type and researched the catalytic combustion characteristics through computer simulation. In this study, we compared detailed homogeneous and heterogeneous chemistry models, and investigated the effects of temperature, equivalence ratio, velocity, entrance diameter of monolithic channel and inlet pressure on methane conversion on the process of methane catalytic combustion. Chou [29] researched the methane catalytic combustion process in monolithic reactor supported by Pt catalyst with multi-step surface reaction mechanism, and verified the simulation results, such as combustion temperature, methane conversion and mole fraction of CO, by comparing with the experimental data at the same operation conditions. Hence the results indicated that multi-step reaction mechanism with adsorption reaction, wall catalytic reaction and desorption reaction, can describe the catalytic combustion process veritably. Chen [30] investigated the catalytic combustion of hydrogen in one channel of the monolithic reactor by using computational fluid dynamics (CFD) software, FLUENT. The detailed reaction kinetics of combustion process in gas phase and catalytic reaction kinetics between gas and solid phase were both considered in the study. The effects of wall heat conductivity coefficient,

†To whom correspondence should be addressed.
E-mail: huangk@seu.edu.cn

inlet velocity and reactor diameter on hydrogen conversion and reaction process were discussed, and the results showed that the reaction process of hydrogen and oxygen in gas phase could not be neglected. Benedettoa [31] built a two-dimensional CFD model of methane catalytic combustion which coupled the fluid flow and chemical reaction process. The reaction rate, methane conversion and temperature in the reactor were discussed under a series of pressures.

The previous researches considered the heat transfer, momentum transfer and mass transfer in the reactor channel. However, the effect of diffusion in the catalyst coating on reaction process was always ignored in the past studies. Zhao [32] studied the performance of monolithic reactor and proved that the diffusion process exists and cannot be neglected in many catalytic reactions occurred in monolithic reactor. Hence, the effect of diffusion on catalytic reaction should be integrated in a multi-scale model for monolithic reactor. In this paper, a novel multi-scale model of methane catalytic combustion on monolithic reactor is built, which contains CFD model (macro-scale) and reaction-diffusion model (meso-scale and micro-scale). The multi-scale model includes mass and heat transfer in the gas phase and contains the reaction-diffusion process inside monolithic catalyst and external diffusion process between gas phase and solid phase. The establishment of multi-scale model of methane catalytic combustion aims to improve the accuracy of simulation and investigates the influences of diffusion, methane concentration, inlet flow velocity and temperature on the methane conversion and reactor performance.

MULTI-SCALE MODEL

1. Monolithic Reactor Model

The monolithic reactor model built by Huang [33] (Fig. 1) was chosen for the simulation of methane catalytic reaction process. The monolithic reactor is supported by washcoat which is composed by 0.5%Pd/γ-Al_2O_3 catalyst. The length and inner diameter of the reactor are 0.075 m and 0.01 m, respectively. Other reactor parameters such as geometric surface area (GSA) and open frontal area (OFA) are shown in Table 3.

According to the gas flow characteristics of the internal channel of a monolithic reactor and the peculiarity and catalyst properties of the methane catalytic reaction, it can be assumed that the flow of gas in the catalyst channel is completely evolutionary laminar; methane and dry air in the reactor channel are ideal gas and the gas distribution in the reactor channel is uniform; all the active sites on the catalyst in the reactor are uniform; the volumetric reaction is ignored in the channel of monolithic reactor because of the low methane concentration.

2. Mathematic Model

Methane catalytic combustion is an extremely complex physical and chemical process in the monolithic reactor; the process includes gas flow, mass and heat transfer between gas phase and catalyst washcoat, chemical reaction process and heat transfer among different channels. When methane and air flow into the monolithic reactor, the chemical reaction occurs rapidly on the catalyst surface. However, the catalyst pore is small and the reaction is very quick; therefore, enormous mass transfer resistance exists during the gas diffusion process. The whole procedure is that reactants undergo the mass diffusion and surface adsorption, and then chemical reaction occurs combined with the active sites; finally, products are back to the gas phase through surface desorption and mass diffusion. Hence, the influence of diffusion on reaction process must be considered in the reactor.

In this study, the multi-scale model of monolithic reactor was built, which includes fluid flow model and porous model coupled by reaction-diffusion model of methane catalytic combustion by using the CFD software. Reaction-diffusion model describes the diffusion behavior and reaction process, which belong to meso-scope and micro-scope, respectively, while the porous model and fluid flow model can represent the flow field of the monolithic reactor, which belongs to macro-scope. Based on the conservation of energy, mass and momentum, the mathematic model can be described by a series of control equations:

For solid phase:

Equation of continuity:

$$\frac{\partial(\phi\rho_g)}{\partial t}+\nabla\cdot(\phi\rho_g\vec{v})=0 \tag{1}$$

Conservation equation of momentum:

$$\frac{\partial(\phi\rho_g\vec{v})}{\partial t}+\nabla\cdot(\phi\rho_g\vec{v}\vec{v})=-\phi\nabla p+\nabla\cdot\phi\bar{\bar{\tau}}+\phi\rho_g\vec{g}+\vec{S} \tag{2}$$

Conservation equation of energy:

$$\frac{\partial[\phi\rho_g E_g+(1-\phi)\rho_{cat}E_s]}{\partial t}+\nabla[\vec{v}(\rho_g E_g+p)] \tag{3}$$

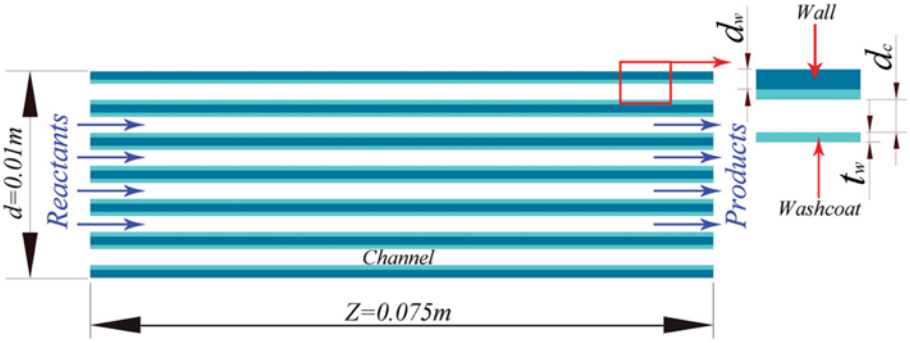

Fig. 1. The physical model of monolithic reactor.

$$= \nabla\left[k_{eff}\nabla T - \left(\sum_{i=1}^{N_r} h_i \vec{J}_i\right) + \overline{\overline{\tau}}\cdot\vec{v}\right] + S_f^h$$

where:

$$k_{eff} = \phi k_g + (1-\phi)k_s \quad (4)$$

Mass conservation equation of each component:

$$\frac{\partial(\phi\rho_g Y_i)}{\partial t} + \nabla\cdot(\phi\rho_g\vec{v}Y_i) = -\phi\nabla\cdot\vec{J}_i + \phi R_i,\ i\in[1, N_r] \quad (5)$$

where:

$$\vec{J}_i = -\rho_g D_{i,m}\cdot\nabla Y_i \quad (6)$$

Stress-strain tensor:

Table 1. Reaction-diffusion model and correlation formulas [34-36]

Parameter	Formula
Continuity equation	$\varepsilon\frac{\partial\rho_g}{\partial t} + \frac{v_r^s}{r^2}\frac{\partial}{\partial r}(r^2\rho_g) = 0$
Species mass balance	$\varepsilon\frac{\partial}{\partial t}(\rho_g Y_i) + \frac{v_r^s}{r^2}\frac{\partial}{\partial r}(r^2\rho_g Y_i) = -\frac{1}{r^2}\frac{\partial}{\partial r}(r^2 j_{i,r}) + \overline{S}_i$
Heat balance	$\left[(1-\varepsilon)Cp_{cat}\rho_{cat} + \varepsilon\rho_g\sum_{i=1}^{n} Y_i Cp_i\right]\frac{\partial T}{\partial t} = -\rho_g\sum_{i=1}^{n} Y_i Cp_i v_r^s\frac{\partial T}{\partial r} - \frac{1}{r^2}\frac{\partial}{\partial r}(r^2 Q_r) + \hat{S}$
Momentum equation	$v_r = \frac{\varepsilon d_0^2}{32\tau\mu}\frac{\partial P}{\partial r}$
Boundary conditions	At the center of particle (r_p=0): $\frac{\partial Y_i}{\partial r} = 0,\ \frac{\partial T}{\partial r} = 0$ At the surface of particle (r_p=d_p/2): $k_{i,g}(Y_i^s - Y_i^f) = -Y_i^s D_{im}\left.\frac{\partial Y_i}{\partial r}\right\|_r - v_r^s\rho_g Y_i^s$ $\lambda\left.\frac{\partial T}{\partial r}\right\|_s - \rho_g Cp_{cat}T^s v_r^s = h_{i,g}(T^f - T^s)$
Gas phase equation of state	$p = \rho_g RT/M$
Definition	$\sum_{i=1}^{n} Y_i = 1$
Heat flux	$Q_r = -\lambda\frac{\partial T}{\partial r}$
Mass source term	$\overline{S}_i = (1-\varepsilon)M_i\rho_{cat}r_{CH_4}$
Heat source term	$\hat{S} = \sum(-\Delta H_{r_k})\cdot r_{CH_4}$
Diffusion coefficient	$D_{i,eff} = \frac{\varepsilon}{\tau}\frac{1}{\frac{1}{D_{i,m}} + \frac{1}{D_{i,k}}}$ $D_{i,k} = 97\frac{d_0}{2}\sqrt{\frac{T}{M_i}}$ $D_{i,m} = \frac{1-Y_i}{M\sum_{\substack{j=1\\ j\neq i}}^{n}\frac{Y_j}{M_j D_{ij}}}$ $D_{ij} = \frac{0.00143\times T^{1.75}}{PM_{ij}^{1/2}\left[(\Sigma_v)_i^{1/3} + (\Sigma_v)_j^{1/3}\right]^2}$
Mass and heat transfer coefficient	$k_{i,g} = \frac{D_{im}Sh_i}{d_p},\ Sh_i = 2 + 0.6Sc_i^{1/3}Re_i^{0.5},\ Sc_i = \frac{\mu_i}{\rho_i D_{im}}\ Re_i = \frac{d_p u\rho_i}{\mu_i},$ $h_{i,g} = \frac{k_{i,g}Nu_i}{d_p},\ Nu_i = 2 + 0.6Pr^{1/3}Re^{0.5}$ $Pr = \frac{Cp_i\cdot\mu_i}{\lambda_i}$

$$\bar{\bar{\tau}} = \mu\left[(\nabla\vec{v} + \nabla\vec{v}^{T}) - \frac{2}{3}\nabla\cdot\vec{v}\bar{\bar{I}}\right] \quad (7)$$

Gas-solid exchange rate:

$$\vec{S} = 150\frac{(1-\phi)^2\mu}{d_p^2\phi^2}\vec{v} + 1.75\frac{\rho_g(1-\phi)|\vec{v}|}{d_p^2\phi}\vec{v} \quad (8)$$

Mass rate of reaction:

$$R_i = M_i\sum_{r=1}^{N_r}\left[(v''_{i,r} - v'_{i,r})\left(k_{f,r}\prod_{j=1}^{N_r}(C_{j,r})^{(\eta'_{j,r}+\eta''_{j,r})}\right)\right] \quad (9)$$

For gas in the monolithic reactor channel:

Equation of continuity:

$$\frac{\partial\rho_g}{\partial t} + \nabla\cdot(\rho_g\vec{v}) = 0 \quad (10)$$

Conservation equation of momentum:

$$\frac{\partial(\rho_g\vec{v})}{\partial t} + \nabla\cdot(\rho_g\vec{v}\vec{v}) = -\nabla p + \nabla\cdot\bar{\bar{\tau}} + \rho_g\vec{g} \quad (11)$$

Conservation equation of energy:

$$\frac{\partial(\rho_g E_g)}{\partial t} + \nabla[\vec{v}(\rho_g E_g + p)] = \nabla\left[k_{eff}\nabla T - \left(\sum_{i=1}^{N_r} h_i\vec{J}_i\right) + \bar{\bar{\tau}}\cdot\vec{v}\right] + S_f^{h'} \quad (12)$$

The reaction-diffusion model and correlation parameters are shown in Table 1. It contains species mass balance equation, heat balance equation, momentum equation, boundary conditions and diffusion parameters. The coupling mechanism of control equations and reaction-diffusion model was described in previous paper [37].

3. Kinetic Model

According to the literature [38-40], so far Pd/γ-Al_2O_3 is the most effective catalyst for methane catalytic combustion. Hurtado [41] studied the intrinsic kinetics of methane catalytic combustion in 0.5% Pd/γ-Al_2O_3 catalyst. Three kinds of models, Different Eley-Rideal model, Langmuir-Hinshelwood model and Mars-van Krevelen model, were compared in the research. Based on the experiment results, the Mars-van Krevelen model (MKV2) proved to be the best intrinsic kinetics of methane catalytic combustion in the research.

Table 2. Parameters of kinetic model [41]

Parameters	Values
k_{10} (mol·bar^{-1}·min^{-1}·g^{-1})	2.5×10^{-3}
k_{20} (mol·bar^{-1}·min^{-1}·g^{-1})	5.6×10^{-2}
k_{30} (mol·bar^{-1}·min^{-1}·g^{-1})	9.3×10^{-5}
Ea_1 (kJ·mol^{-1})	55.1
Ea_2 (kJ·mol^{-1})	21.1
Ea_3 (kJ·mol^{-1})	106.6

Table 3. Parameters of multi-scale model

Parameters	Values
Gas-mixture	
Mass heat capacity ($C_{p,g}$/kJ·kg·K^{-1})	Mixing-law
Gas density (ρ_g/kg·m^{-3})	Incompressible-ideal-gas
Gas thermal conductivity (k_g/W·m^{-1}·K^{-1})	Ideal-gas-mixing-law
Gas viscosity (μ/Pa·s)	Ideal-gas-mixing-law
Solid phase	
Pore diameter (d_0/m)	1.55×10^{-8}
Particle curvature factor (τ)	4
Catalyst density (ρ_{cat}/kg·m^{-3})	2380
Catalyst thermal conductivity (k_s/W·m^{-1}·K^{-1})	0.2514
Reactor parameters	
Inlet boundary	Velocity inlet
Outlet boundary	Pressure outlet
Wall boundary	No slip with 0.002 m
Pressure (kPa)	100
Inlet gas flow (ml·min^{-1})	200
Bulk concentration of CH_4	0.4%
Transport & reaction	By UDF
Catalyst length (Z/m)	0.075
Porosity (ϕ)	0.43
Bed diameter (d/m)	0.01
Catalyst wall thickness (t_w/mm)	0.3
Channel diameter (d_c/mm)	1.2
GSA (m^2/m^3)	1481
OFA (%)	44.5
Convergence criteria	10^{-3}

Table 4. Mole heat capacity of reaction components ($C_p^0/R=A+BT+CT^2+DT^3+ET^3$; $J\cdot mol^{-1}K^{-1}$)

Component	a_i	$b_i\times10^{-3}$	$c_i\times10^{-5}$	$d_i\times10^{-8}$	$e_i\times10^{-11}$
CH_4	1.918	−1.094	87.045	−52.343	0
CO_2	3.259	1.356	1.502	−2.374	1.056
O_2	3.630	−1.794	0.658	−0.601	0.179
H_2O	4.395	−4.186	1.405	−1.564	0.632

Table 5. Physical property and mole enthalpy of species

Component	M_i (kg/kmol)	Diffusion volume	$\Delta H_{f\,298}$ (kJ/mol)
CH_4	16	12.0	−74.81
CO_2	44	26.9	−393.51
O_2	32	16.3	0
H_2O	18	13.1	−136.31

$$CH_4+O_2\rightarrow CO_2+H_2O \quad \Delta H_{298K}=-802\ kJ/mol \tag{13}$$

Intrinsic kinetics model:

$$r_{CH_4}=\frac{k_1k_2P_{CH_4}P_{O_2}}{k_1P_{O_2}+2k_2P_{CH_4}+(k_1k_2/k_3)P_{CH_4}P_{O_2}} \tag{14}$$

$$k_i=k_{i0}\exp\left[-Ea_i\left(\frac{1}{RT}-\frac{1}{RT_m}\right)\right] \tag{15}$$

Here, P_{CH_4} and P_{O_2} denote the pressures of methane and oxygen, respectively. k_i denotes the constant of the reaction rate. Ea_i denotes the activation energy. R is the gas constant.

SIMULATION METHODS

1. Model Parameters

The parameters of the reaction kinetics and multi-scale model are listed in Table 2 and Table 3, respectively. The heat capacity data of reaction components and physical properties of species are in Tables 4 and 5, respectively.

2. Modelling Method

The multi-scale model of monolithic reactor was simulated in the FLUENT software. After defining the model values, material parameters, boundary conditions and operation conditions, the two-dimensional geometric reactor model was generated by pre-process software GAMBIT, and then imported into FLUENT software. The governing equation was dispersed by first-order upwind difference scheme by using C programming language, and coupled with the CFD by user-defined-function (UDF).

3. Model Validation

The 10,000 cells are adequate for the above founded multi-scale reactor model through the analysis of grid independence in Fig. 2. The reaction-diffusion model and the porous model were proved by previous scholars, respectively [42-44]. To validate the correction of the monolithic reactor multi-scale model, the simulated results and the experiment data from Huang [33] are compared in Fig. 3. As shown in Fig. 3, the methane conversion changes with the increase of temperature, Case 1 denotes dataderived from Huang [30]; Case 2 is the simulated results of monolithic reactor multi-scale model; Case 3 represents monolithic reactor model without diffusions. From the Fig. 3, the relative error of Case 2 is less than that of Case 3 after comparing the simulated results with the experiment data (Case 1). Therefore, these results demonstrate that the multi-scale model can describe the monolithic reactor fairly well.

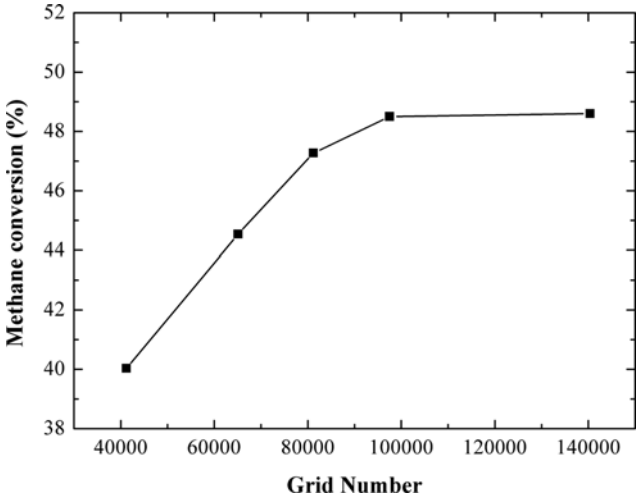

Fig. 2. The influence of grid number on simulation result.

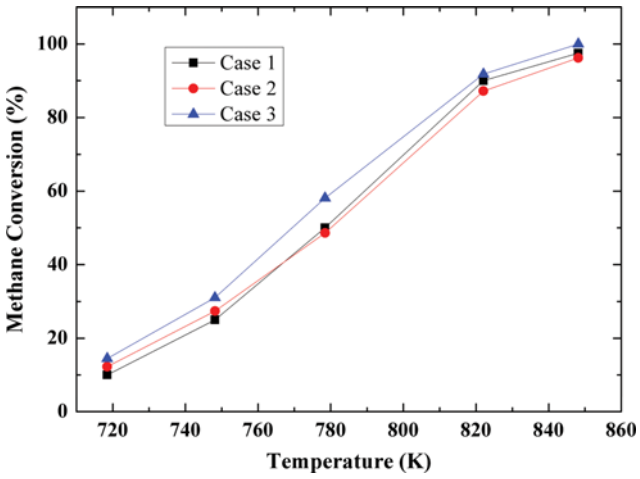

Fig. 3. The comparison between simulated data and experiment data (case 1: experiment data, case 2: CFD coupled without diffusion equations, case 3: multi-scale model of monolithic reactor).

RESULTS AND DISCUSSION

To investigate the changing regularity of gas flow and temperature at the end of the catalyst reactor, the pipe is extended according to the real situation. The inlet temperature and methane bulk concentration are set to 778 K and 1%, respectively. The original reactant includes methane and dry air, and the inlet flow rate is 800 mL/min. The effects of diffusion were investigated through the comparison of multi-scale model with pure CFD model coupling reaction kinetics model without diffusion equations. The methane conversion can be computed with the following formula:

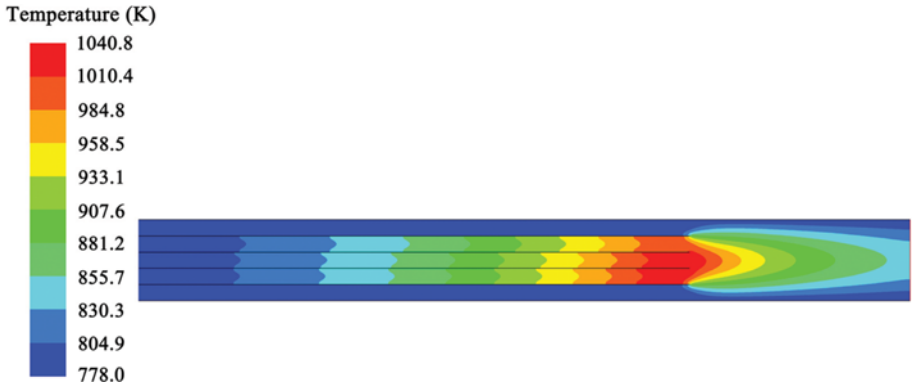

Fig. 4. The contour of temperature in the monolithic reactor.

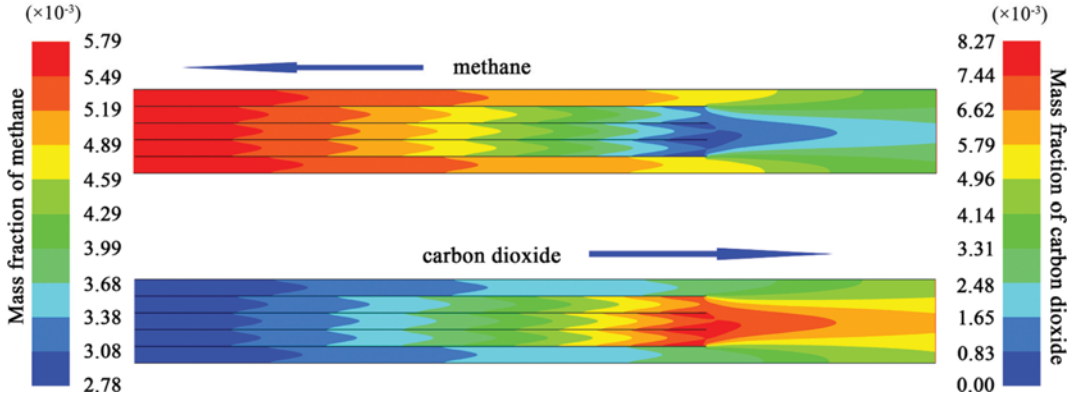

Fig. 5. The contours of methane and carbon dioxide in the reactor.

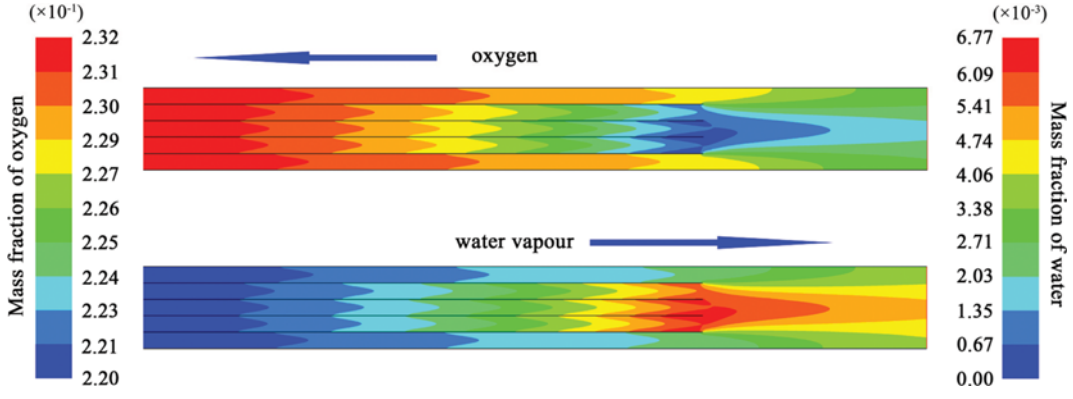

Fig. 6. The contours of oxygen and water vapour in the reactor.

$$x_{CH_4} = \frac{F_{0CH_4} - F_{CH_4}}{F_{0CH_4}} \quad (16)$$

1. Parameter Distributions of Monolithic Reactor

Parameter distributions of monolithic reactor, such as pressure, temperature and each component's concentration, can be described clearly in the multi-scale model. The pressure drop of the monolithic reactor is only 2.5 Pa through computation of the multi-scale model, hence compared to other kinds of reactors, it has enormous advantage at pressure drop. The temperature distribution and each component's concentration distribution are shown in Fig. 4, Fig. 5 and Fig. 6 respectively.

Temperature distribution contour of monolithic reactor is exhibited in Fig. 4, which shows that the highest temperature is above 1,000 K at the reactor outlet. The reason for this phenomenon is that methane catalytic combustion is a rapid highly exothermic reaction, the radial heat transfer is very little, and the gas flow takes heat to the reactor outlet. The temperature variation maintains relative stabilization in two channels next to the reactor wall because of the rapid heat exchange between reactor wall and catalyst. Fig. 5 and

Fig. 6 describe the distribution contours of methane, carbon dioxide, oxygen and water, respectively. Reactants, methane and oxygen, decrease along the axial direction of the reactor, and the mass fraction of methane is close to 0.003 at the reactor outlet. Productions, carbon dioxide and water vapor, increase along the axial direction of the monolithic reactor. The temperature distribution and each component's concentration distribution at outlet are also shown in Fig. 4, Fig. 5 and Fig. 6, respectively.

2. Influence of Diffusion on the Monolithic Reactor

Two kinds of temperature distribution contours and each component's concentration contours are shown in Fig. 7, Fig. 8, Fig. 9, Fig. 10 and Fig. 11 by using the different models for simulation; case 1 is the monolithic reactor multi-scale model and case 2 is the pure CFD model without diffusion resistance. The highest tem-

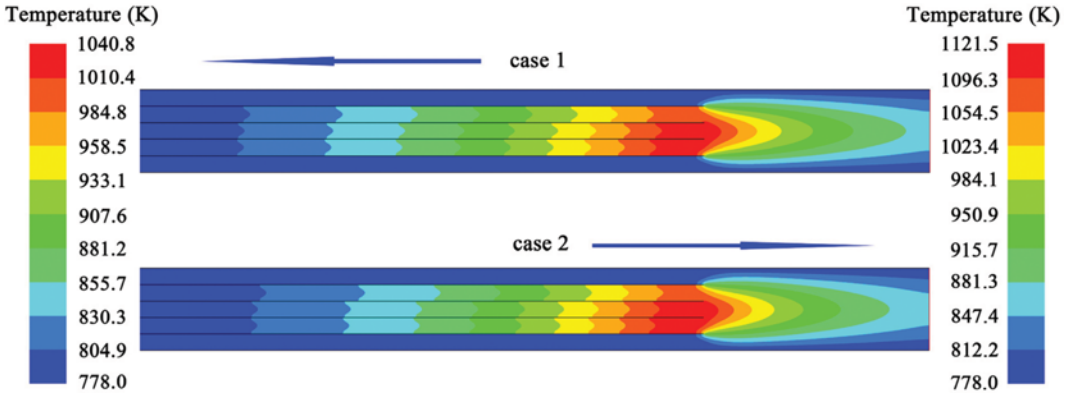

Fig. 7. The temperature distribution contours in the monolithic reactor (case 1: the multi-scale model, case 2: pure CFD model without diffusion equations).

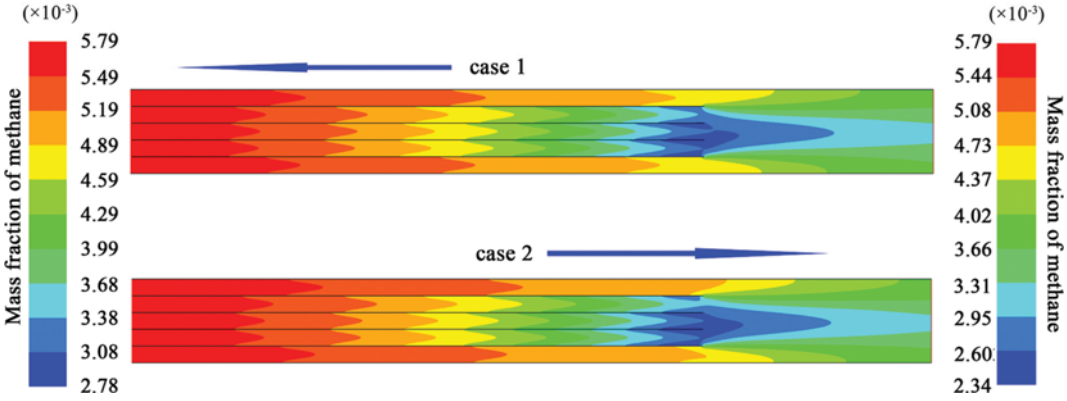

Fig. 8. Distribution contours of CH_4 in the monolithic reactor (case 1: the multi-scale model, case 2: pure CFD model without diffusion equations).

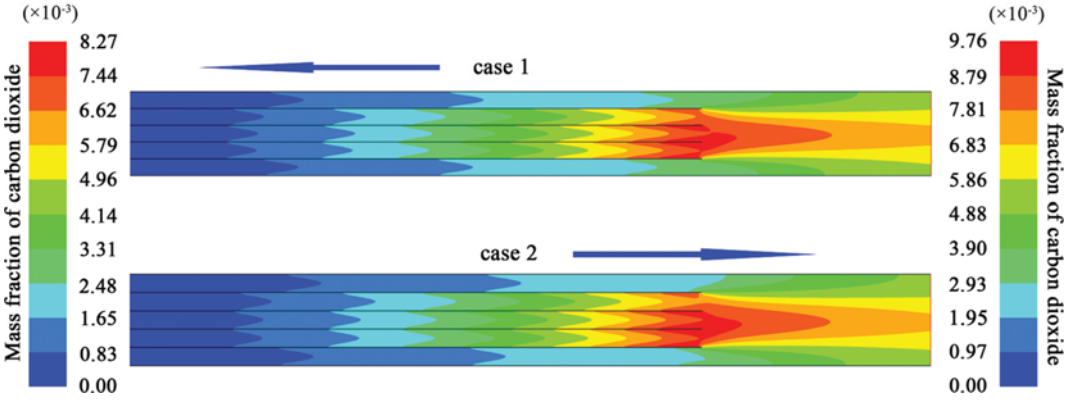

Fig. 9. Distribution contours of CO_2 in the monolithic reactor (case 1: the multi-scale model, case 2: pure CFD model without diffusion equations).

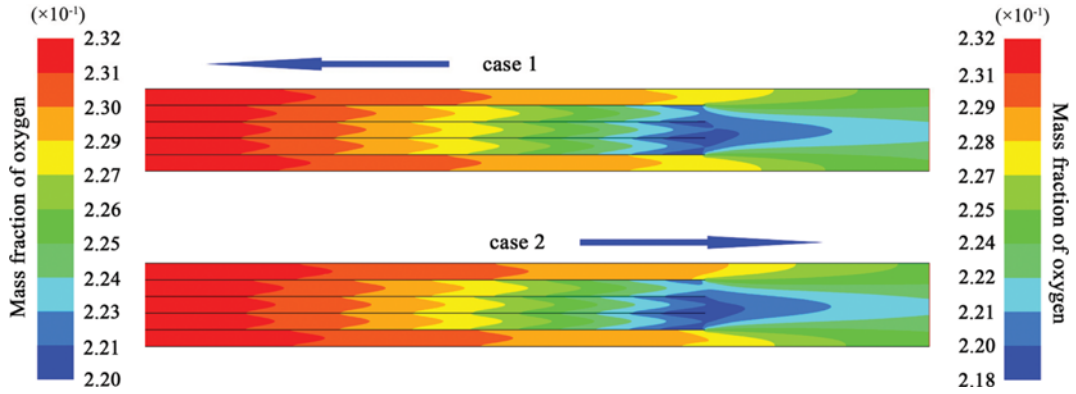

Fig. 10. Distribution contours of O_2 in the monolithic reactor (case 1: the multi-scale model, case 2: pure CFD model without diffusion equations).

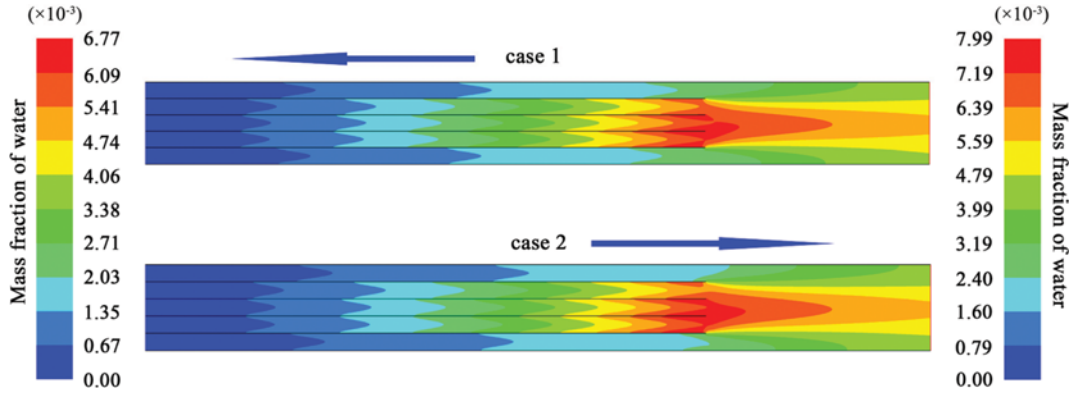

Fig. 11. Distribution contours of H_2O in the monolithic reactor (case 1: the multi-scale model, case 2: pure CFD model without diffusion equations).

perature in case 1 is 1,040.8 K, while the highest temperature in case 2 is 1,121.5 K. The reason for this phenomenon is that the diffusion resistance is neglected in case 2, which leads to faster methane reaction rate. Therefore, the quantity of heat production in case 2 is more than case 1.

The distribution contours of methane, carbon dioxide, oxygen and water vapor in two kinds of models are exhibited in Fig. 8, Fig. 9, Fig. 10 and Fig. 11. The lowest mass fraction of methane is 0.00278 in case 1, while that in case 2 is 0.00234 in the Fig. 8. It has similar regularity about mass fraction of oxygen, carbon dioxide and water vapor in Fig. 9, Fig. 10 and Fig. 11. Methane catalytic combustion is a rapid reaction, but diffusion process is slow, hence, the rate-controlling step of the reaction-transport process is diffusion rate. In conclusion, the process of methane catalytic combustion is controlled by the diffusion resistance; the influence of diffusion cannot be neglected in the process of methane catalytic combustion.

3. Influence of Methane Concentration on the Monolithic Reactor

The effect of methane concentration on methane conversion and temperature distribution in the monolithic reactor, is considered as shown in Fig. 12 and Fig. 13, respectively. Different methane bulk concentrations (1.0%, 1.1%, 1.2% and 1.3%) are simulated at the same gas flow rate (800 mL/min) and inlet temperature (778 K). Fig. 13 describes the temperature distribution of the monolithic reactor at the different methane bulk concentrations. The temperature increases with increasing the methane bulk concentration. When the volume fraction of methane reaches 1.3%, the temperature reaches 1,350 K at the monolithic reactor outlet, while it is only 1,040 K at 1.0%. Consequently, methane catalytic combustion reaction is a

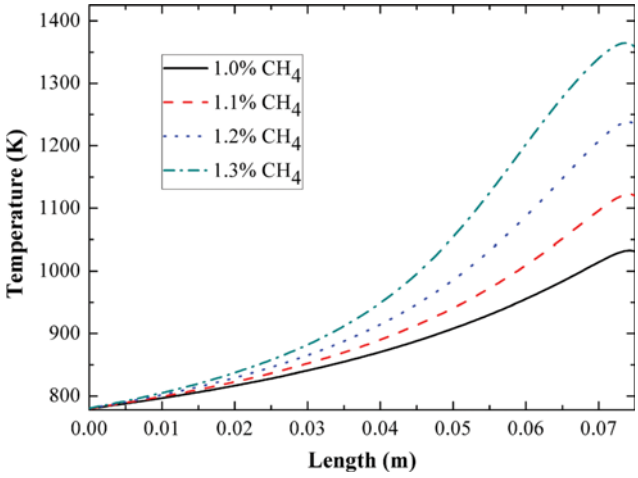

Fig. 12. The effect of different methane concentrations on temperature of channel.

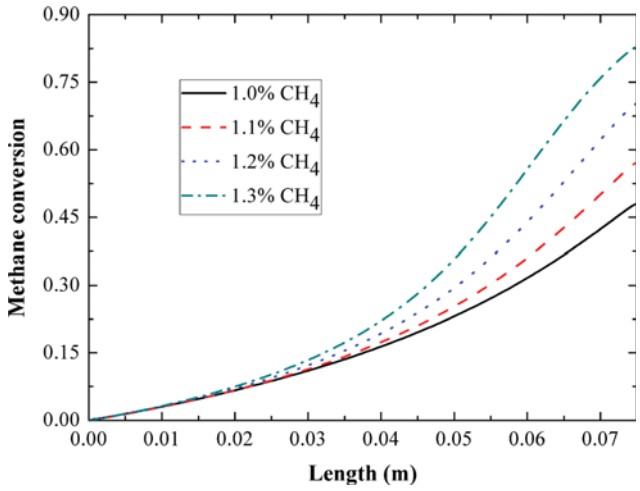

Fig. 13. Distribution of methane conversion along the axial in different methane concentrations.

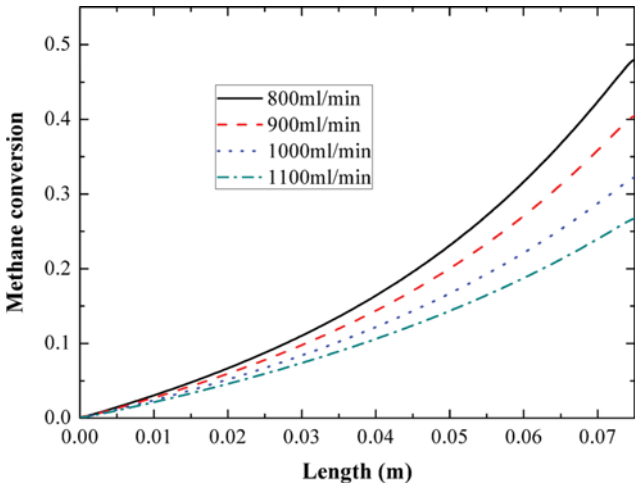

Fig. 15. The effect of different flow rates on methane conversion in the reactor.

strongly exothermal reaction.

The effect of methane bulk concentration on methane conversion is shown in Fig. 13. The methane conversion increases with increasing methane volume fraction. The methane conversion is only 0.48 at the outlet when methane volume fraction is 1.0%, while it reaches 0.86 at 1.3%. The differences of methane conversion and temperature among four concentrations, are very small within 0.02 m of the reactor inlet. The reason for this phenomenon is that the reaction rate is small and increases slightly with the increase of methane concentration at the reactor inlet. However, the impact of concentration and temperature on the process of catalytic reaction becomes more and more prominent after 0.02 m in the reactor inlet. Therefore, it can increase the methane conversion by increasing the volume fraction of methane appropriately; meanwhile, catalyst deactivation due to excessive heat should be avoided carefully.

4. Influence of Flow Rate on the Monolithic Reactor

The influence of different flow rates (800 mL/min, 900 mL/min, 1,000 mL/min and 1,100 mL/min) on temperature and methane conversion is shown in Fig. 14 and Fig. 15 at the same methane concentration and inlet temperature. The temperature and methane conversion increase along with the direction of axial in all flow rate conditions, because the contact time increases as the proceeding of catalytic reaction. The highest temperature in the reactor decreases with the increase of gas flow rate from Fig. 14. The highest temperature appears at the monolithic reactor outlet, and the highest temperature is 1,030 K at 800 mL/min, while it is 925 K at 1,100 mL/min. A similar phenomenon occurs at methane conversion with the increase of gas flow rate in Fig. 15. The methane conversion is 0.48 at 800 mL/min at the reactor outlet, while it is only 0.26 at 1,100 mL/min. With the increase of flow rate, the contact time of reactants and catalyst decreases; most of the reactants and heat derived from the reaction leave the reactor rapidly, and that is the reason for the decrease in methane conversion and the temperature.

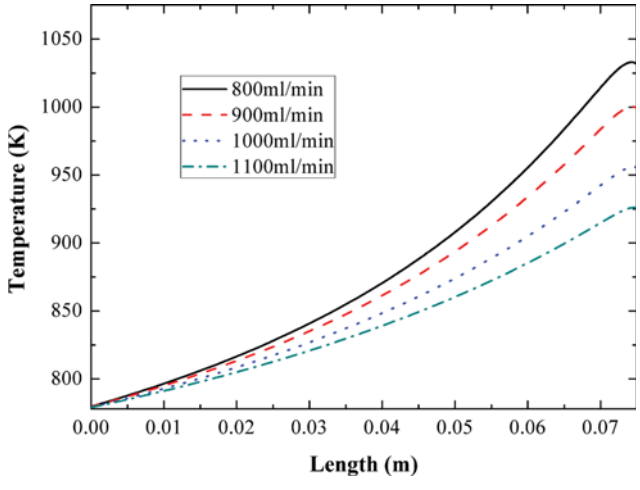

Fig. 14. The temperature distribution along the flow direction at different flow rates.

CONCLUSIONS

A novel multi-scale model of methane catalytic combustion solved by FLUENT was built in the monolithic reactor. The validity of the multi-scale model was verified through the analysis of grid independence and the experiment data from Huang [30], and the multi-scale model achieved better simulation accuracy than the pure CFD model, and it was also better than previous work. The distribution of temperature and each component's mass fraction were calculated in all reactor channels by using the multi-scale model. Based on the multi-scale model and pure CFD model without diffusion under the same boundary conditions, the temperature distribution and mass fraction of methane, carbon dioxide, oxygen and water vapour were analyzed, and comparison of two kinds of models reveals that the diffusion process in the monolithic reactor cannot be neglected at the process of methane catalytic combustion. Furthermore, the effects of methane concentration and gas flow rate on the temperature distribution and methane conversion were discussed by the simulated results of the monolithic reactor multi-scale model. The optimal operating methane concentration

and flow rate can be gained by using the multi-scale model according to the real situations.

ACKNOWLEDGEMENT

This work was supported by the National Natural Science Foundation of China (No. 21576049), the Fundamental Research Funds for the Central Universities (No. 2242016K40082).

NOMENCLATURE

$C_{p,g}$: mass specific heat of the gas phase [J·kg^{-1}·K^{-1}]
Cp_{cat} : mass heat capacity of catalyst [kJ·kg^{-1}·K^{-1}]
Cp_i : mass heat capacity of i component [kJ·kg^{-1}·K^{-1}]
d_h : hydraulic diameter of monolith channel [mm]
d_0 : catalyst average diameter [mm]
$D_{i,eff}$: effective diffusion coefficient of the ith component [m^2·s^{-1}]
D_{im} : Fick diffusion coefficient of the ith component [m^2·s^{-1}]
D_{ik} : Knudsen diffusion coefficient of the ith component [m^2·s^{-1}]
Ea_i : activation energy [K]
E_g : total fluid energy [kg·m^2·s^{-2}]
E_s : total solid medium energy [kg·m^2·s^{-2}]
f : fanning coefficient
g : gravitational acceleration [m^2·s^{-2}]
GSA : geometric surface area [m^2·m^{-3}]
$h_{i,g}$: heat transfer coefficient [W·m^{-2}·K^{-1}]
H_i : enthalpy of the ith component [kJ·kg^{-1}]
h_i : species enthalpy of formation [kJ·kg^{-1}]
$\overline{\overline{I}}$: identity matrix
$J_{i,r}$: mass diffusion flux [kg·m^{-2}·s^{-1}]
$\vec{J}_i$: diffusion flux of species i [kg·m^{-2}·s^{-1}]
$k_{i,g}$: mass transfer coefficient [m/s]
k_i : intrinsic rate constant of the ith step based on species mass fraction [mol·kg$_{cat}^{-1}$·h^{-1}·Pa^{-1}]
k_f : fluid phase thermal conductivity [W·s^{-1}·K^{-1}]
k_s : solid medium thermal conductivity [W·s^{-1}·K^{-1}]
k_{eff} : effective thermal conductivity of the medium [W·s^{-1}·K^{-1}]
M : mixture fluid molar mass [kg·kmol^{-1}]
M_i : molar mass of the ith component [kg·kmol^{-1}]
M_0 : mixture fluid molar mass at bulk [kg·kmol^{-1}]
N_r : number of chemical species
OFA : open frontal area
P : pressure [kPa]
P_r : Prandtl number
Q_r : heat flux [J·m^{-2}·s^{-1}]
r_0 : catalyst particle radius [m]
Re_i : Reynolds number of the ith component
R : ideal gas constant [kJ·kmol·K^{-1}]
Sh_i : Sherwood number of the ith component
Sc : Schmidt number
$\overline{S}_i$: mass source of the ith component of single model [kg·m^{-3}·s^{-1}]
$\hat{S}_i$: heat source of single model [J·m^{-3}·s^{-1}]
s : surface conditions
$\vec{S}$: source term for the momentum equation [kg·m^{-3}·s^{-1}]
S_f^h : fluid enthalpy source term [J·m^{-3}·s^{-1}]
T : temperature [K]
T^s : temperature at particle outer surface [K]
t_w : monolith wall thickness [m]
u : apparent gas velocity [m·s^{-1}]
$\vec{v}$: gas velocity vector [m·s^{-1}]
$\vec{v}^T$: transpose of velocity vector [m·s^{-1}]
$v'_{i,r}$: stoichiometric coefficient for reactant i in the rth reaction
$v''_{i,r}$: stoichiometric coefficient for product i in the rth reaction
$\eta'_{i,r}$: rate exponent for reactant species j in the rth reaction
$\eta''_{i,r}$: rate exponent for product species j in the rth reaction
v_r^s : gas velocity at particle outer surface [m·s^{-1}]
Y_i : mass fraction of the ith component
Y_i^s : mass fraction of the ith component at the particle outer surface
$Y_{i,0}$: mass fraction of the ith component at bulk
ε : catalyst porosity
ρ_g : mixture gas density [kg·m^{-3}]
ρ_0 : mixture fluid density at bulk [kg·m^{-3}]
ρ_{cat} : real catalyst density [kg·m^{-3}]
ρ_i : the ith component density [kg·m^{-3}]
μ : mixture fluid viscosity [Pa·s^{-1}]
μ_i : viscosity of species i [Pa·s^{-1}]
$(\Sigma_v)_i$: diffusion volume of the ith component [m^3·mol^{-1}]
λ : thermal conductivity [W·s^{-1}·K^{-1}]
λ_i : thermal conductivity coefficient of the ith component [W·s^{-1}·K^{-1}]
η : effectiveness factor of the ith step
ϕ : medium porosity
τ : curvature factor
$\overline{\overline{\tau}}$: shear stress of gas phase
Nu_i : Nusselt number of the ith component

REFERENCES

1. J. W. Li, J. J. Zhang, Z. G. Lei and B. H. Chen, *Energy Fuel*, **26**, 443 (2012).
2. J. Hu, R. Hu, R. Ding, J. Chen and Y. Zhang, *Catal. Commun.*, **21**, 38 (2012).
3. G. H. Zhu, J. Y. Han, D. Y. Zemlyanov and F. H. Ribeiro, *J. Am. Chem. Soc.*, **126**, 9896 (2004).
4. K. M. Santhosh, M. H. Aguirre, A. Weidenkaff and D. Ferri, *J. Phys. Chem. C.*, **114**, 9439 (2010).
5. B. Wang, Z. F. Qin and G. F. Wang, *Catal. Lett.*, **143**, 411 (2013).
6. Y. G. Zhang, Z. F. Qin and G. F. Wang, *Appl. Catal. B-Environ.*, **129**, 172 (2013).
7. N. Jodeiri, J. P. Mmbaga and L. Wu, *Comput. Chem. Eng.*, **39**, 47 (2012).
8. B. H. Yue, R. X. Zhou and X. M. Zheng, *Fuel Process. Technol.*, **8**, 728 (2008).
9. R. F. Hick, H. H. Qi and M. L. Young, *J. Catal.*, **122**, 280 (1990).
10. K. Persson, P. O. Thevenin and K. Jansson, *Appl. Catal. A-Gen.*, **249**, 165 (2003).
11. L. H. Xiao, K. P. Sun and X. L. Xu, *Catal. Commun.*, **6**, 796 (2005).
12. F. J. Aires, S. Cadete, I. Kurzina, G. G. Cervantes and J. C. Bertolini, *Catal. Today*, **117**, 518 (2006).

13. S. Colussi, A. Trovarelli, C. Cristiani and L. Lietti, *Catal. Today*, **180**, 124 (2012).
14. A. Ersson, K. Persson and I. K. Adu, *Catal. Today*, **112**, 157 (2006).
15. H. Arai, T. Yamada and K. Eguchi, *Appl. Catal.*, **26**, 265 (1986).
16. I. Rossetti and L. Forni, *Appl. Catal. B-Environ.*, **33**, 345 (2001).
17. X. G. Ren, J. D. Zheng and Y. J. Song, *Catal. Commun.*, **9**, 807 (2008).
18. A. J. Zarur and J. Y. Ying, *Nature*, **403**, 65 (2000).
19. J. Cheng, H. L. Wang and Z. P. Hao, *Catal. Commun.*, **9**, 690 (2008).
20. P. Reyes, A. Figueroa, G. Pecchi and J. L. Fierro, *Catal. Today*, **62**, 209 (2000).
21. S. R. G. Carrazan, R. Mateos and V. Rivesa, *Catal. Today*, **112**, 161 (2006).
22. S. Irandoust and B. Andersson, *Monolithic Catalysts for Nonautomobile Applications Catal Rev Sci Eng.*, **30**, 341 (1988).
23. S. Su and A. Jenny, *Fuel*, **85**, 1201 (2006).
24. P. Marín, M. Hevia, S. Ordóñez and F. V. Díez, *Catal. Today*, **105**, 701 (2005).
25. S. R. Shabanian, M. Rahimi, A. Amiri, S. Sharifnia and A. A. Alsairafi, *Korean J. Chem. Eng.*, **29**, 1531 (2012).
26. B. Chalermsinsuwan, D. Gidaspow and P. Piumsomboon, *Korean J. Chem. Eng.*, **30**, 963 (2013).
27. B. Chalermsinsuwan, T. Thummakul, D. Gidaspow and P. Piumsomboon, *Korean J. Chem. Eng.*, **31**, 350 (2014).
28. C. H. Hwang and C. E. Lee, *Fuel*, **83**, 987 (2004).
29. C. P. Chou, Y. Jyh, H. Greg and S. William, *Combust. Sci. Technol.*, **150**, 1: 27 (2000).
30. J. J. Chen, L. F. Yan and W. Y. Song, *Reac. Kinet. Mech. Catal.*, **113**, 19 (2013).
31. A. Benedetto, G. Landi and V. Sarli, *Catal. Today*, **197**, 206 (2012).
32. Y. Zhao, Y. F. Zheng and F. Xin, *Chem. Reac. Eng. Technol.*, **20**, 357 (2004).
33. J. J. Huang, Z. G. Jia and F. Y. Liu, *Industrial Catalysis*, **5**, 23 (2013).
34. S. Vaishali, S. Roy and P. L. Mills, *Chem. Eng. Sci.*, **63**, 5107 (2008).
35. C. R. Wilke, *Chem. Eng. Prog.*, **46**, 95 (1950).
36. K. R. Rout, J. Solsvik and A. K. Nayak, *Chem. Eng. Sci.*, **66**, 4111 (2011).
37. K. Huang, S. Lin, J. J. Wang and Z. H. Luo, *J. Industrial Eng. Chem.*, **29**, 172 (2015).
38. Y. Ozawa, Y. Tochihara, M. Nagai and S. Omi, *Catal. Commun.*, **4**, 87 (2003).
39. P. Reyes, A. Figueroa, G. Pecchi and J. L. G. Fierro, *Catal. Today*, **62**, 209 (2000).
40. S. Guerrero, P. Araya and E. E. Wolf, *Appl. Catal. A-Gen.*, **298**, 243 (2006).
41. P. Hurtado, S. Ordóñez, S. Herminio and V. Fernando, *Appl. Catal. B-Environ.*, **51**, 229 (2004).
42. Y. Q. Zhuang, X. Gao, Y. P. Zhu and Z. H. Luo, *Powder Technol.*, **221**, 419 (2012).
43. X. M. Chen, J. Dai and Z. H. Luo, *Particuology*, **11**, 703 (2013).
44. G. Q. Chen, Z. H. Luo and X. Y. Lan, *Chem. Eng. J.*, **228**, 352 (2013).